REDUCTION OF NUMERICAL DISPERSION OF ADI-FDTD METHOD WITH QUASI ISOTROPIC SPATIAL DIFFERENCE SCHEME

Yilong Zhang[*], Donglin Su, and Feijiao Liu

Department of Electronics and Information Engineering, Beihang University, Beijing 100191, China

Abstract—In this paper, the difference scheme of the alternating-direction-implicit finite-difference time-domain (ADI-FDTD) method is replaced by the quasi isotropic (QI) spatial difference scheme to improve its numerical dispersion characteristics. The unconditional stability advantage of QI-ADI-FDTD is analytically proven and numerically verified. The numerical dispersion of the novel method can be dramatically reduced by choosing proper weighting factor. An example is simulated to demonstrate the accuracy and efficiency of the proposed method.

1. INTRODUCTION

The finite-difference-time-domain (FDTD) method and its enhanced methods [1–8] are widely used in modeling electromagnetic problems due to their simpleness in updating equations and easiness in numerical implementation [9–14]. Constrained by the Courant-Friedrichs-Lewy (CFL) condition, however, its maximum time step is limited by the minimum cell size, which seriously affects its computational efficiency when fine meshes are required in the object under analysis [15].

To overcome this shortage, several time-domain techniques have been developed including ADI-FDTD method [15]. At the same time of achieving unconditionally stable advantage, ADI-FDTD method gains worse numerical dispersion characteristics than traditional FDTD method, which means its time size is determined by the computational accuracy rather than the CFL condition. Depending on frequency and propagation direction, its phase velocity error leads to the accumulation of phase error and consequently results in computational inaccuracy.

* Corresponding author: Yilong Zhang (zhang_yi_l@sina.com).

To ameliorate the dispersion performance of ADI-FDTD method, considerable attempts have been made. Wang et al. [16] proposed a parameter-optimized (PO) ADI-FDTD method with two additional coefficients, and subsequently, Fu and Tan [17] extended this method with (2, 4) stencil. Similarly, a dispersion-optimized (DO) ADI-FDTD method [18] with several controlling parameters was presented. Juntunen and Tsiboukis [19] introduced artificial anisotropy to reduce the numerical dispersion of the traditional FDTD method, and it was implemented in ADI-FDTD method by Zheng and Leung [20]. Recently, Zhang et al. [21] further extended the artificial anisotropy revision method to higher order ADI-FDTD. Meanwhile, the split-step approach [22] and locally-one-dimensional (LOD) FDTD methods [23] were developed, of which the latter can be considered as a special case of the former. Later, high-order split-step FDTD methods in 2-D [24] and 3-D [25, 26] were presented. Basing on [23], arbitrary-order 3-D LOD-FDTD approach was presented by Liu et al. [27].

As a space point representing electromagnetic field component interacts with all the field points in the vicinity, which cannot be perfectly estimated by only two points, the numerical dispersion results mainly from the second-order central-difference approximation process of the differentiation operation and it is widely believed to be the primary source of computational error of ADI-FDTD method [21]. Basing on, I. S. Koh et al. [28] introduced a novel explicit scheme to reduce the numerical dispersion of FDTD method. In this paper, a similar method is extended to ADI-FDTD, namely, the QI-ADI-FDTD method. To furthest approximate the spatial differentiation, QI-ADI-FDTD samples field points in a quasi isotropic (QI) fashion. A general QI-ADI-FDTD formulation can be achieved in 3 procedures: 1) replace the spatial second-order central-difference scheme in the numerical formulation of ADI-FDTD by the weighted QI difference scheme; 2) determine the weighting factor to minimize the numerical dispersion fluctuation of QI-ADI-FDTD with simple algebraic manipulation such as averaging; 3) revise the electromagnetic attributes in the whole analyzing area to overall remove the numerical dispersion and utmostly approach the exact phase velocity.

In this paper, the detailed procedures to complete the QI-ADI-FDTD formulation are given, with stability analysis and numerical dispersion relationship analytically provided. Additionally, the numerical dispersion characteristics of QI-ADI-FDTD method are detailed investigated, with comparisons to that of the conventional ADI-FDTD method. Finally, a numerical experiment is presented to demonstrate the computational accuracy and efficiency of the proposed method.

2. NUMERICAL FORMULATION OF QI-ADI-FDTD

2.1. Numerical Formulation

Unlike the finite-difference (FD) scheme of conventional ADI-FDTD shown in Figure 1(a), in which only field components H_x along y-axis and H_y along x-axis, in line with E_z, contribute to the iterative equation of field component E_z, that of QI-ADI-FDTD takes all possible related electromagnetic field components in the vicinity into consideration, and comes into a weighted summation difference scheme. Figure 1(b) illustrates the involved field points of the iterative equation of field component E_z. It can be intuitively observed that with quasi omnidirectional field points employed in the FD approximation, QI-ADI-FDTD tends to decrease the anisotropy caused by unidirectional FD approximation.
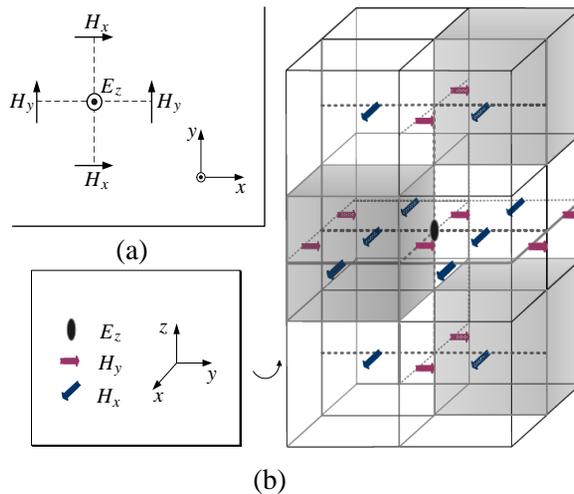

Figure 1. Graphic depiction of the electromagnetic field spatial points involved in two FD approximation schemes in three dimensions. (a) Field components used in the FD approximation of conventional ADI-FDTD method. (b) Field components used in the FD approximation of the QI-ADI-FDTD method.

Consider a linear, lossless, isotropic and non-dispersive medium with permittivity ε and permeability μ. The numerical formulation of the QI-ADI-FDTD method for a full 3-D wave is presented in (1) and (2).

⟨First procedure⟩

$$\frac{E_x^{n+1/2} - E_x^n}{\Delta t/2} = \frac{1}{\varepsilon}\left(\delta_y H_z^n - \delta_z H_y^{n+1/2}\right)_{\bar{i},j,k} \tag{1a}$$

$$\frac{E_y^{n+1/2} - E_y^n}{\Delta t/2} = \frac{1}{\varepsilon}\left(\delta_z H_x^n - \delta_x H_z^{n+1/2}\right)_{i,\bar{j},k} \tag{1b}$$

$$\frac{E_z^{n+1/2} - E_z^n}{\Delta t/2} = \frac{1}{\varepsilon}\left(\delta_x H_y^n - \delta_y H_x^{n+1/2}\right)_{i,j,\bar{k}} \tag{1c}$$

$$\frac{H_x^{n+1/2} - H_x^n}{\Delta t/2} = \frac{1}{\mu}\left(\delta_z E_y^n - \delta_y E_z^{n+1/2}\right)_{i,\bar{j},\bar{k}} \tag{1d}$$

$$\frac{H_y^{n+1/2} - H_y^n}{\Delta t/2} = \frac{1}{\mu}\left(\delta_x E_z^n - \delta_z E_x^{n+1/2}\right)_{\bar{i},j,\bar{k}} \tag{1e}$$

$$\frac{H_z^{n+1/2} - H_z^n}{\Delta t/2} = \frac{1}{\mu}\left(\delta_y E_x^n - \delta_x E_y^{n+1/2}\right)_{\bar{i},\bar{j},k} \tag{1f}$$

⟨Second procedure⟩

$$\frac{E_x^{n+1} - E_x^{n+1/2}}{\Delta t/2} = \frac{1}{\varepsilon}\left(\delta_y H_z^{n+1} - \delta_z H_y^{n+1/2}\right)_{\bar{i},j,k} \tag{2a}$$

$$\frac{E_y^{n+1} - E_y^{n+1/2}}{\Delta t/2} = \frac{1}{\varepsilon}\left(\delta_z H_x^{n+1} - \delta_x H_z^{n+1/2}\right)_{i,\bar{j},k} \tag{2b}$$

$$\frac{E_z^{n+1} - E_z^{n+1/2}}{\Delta t/2} = \frac{1}{\varepsilon}\left(\delta_x H_y^{n+1} - \delta_y H_x^{n+1/2}\right)_{i,j,\bar{k}} \tag{2c}$$

$$\frac{H_x^{n+1} - H_x^{n+1/2}}{\Delta t/2} = \frac{1}{\mu}\left(\delta_z E_y^{n+1} - \delta_y E_z^{n+1/2}\right)_{i,\bar{j},\bar{k}} \tag{2d}$$

$$\frac{H_y^{n+1} - H_y^{n+1/2}}{\Delta t/2} = \frac{1}{\mu}\left(\delta_x E_z^{n+1} - \delta_z E_x^{n+1/2}\right)_{\bar{i},j,\bar{k}} \tag{2e}$$

$$\frac{H_z^{n+1} - H_z^{n+1/2}}{\Delta t/2} = \frac{1}{\mu}\left(\delta_y E_x^{n+1} - \delta_x E_y^{n+1/2}\right)_{\bar{i},\bar{j},k} \tag{2f}$$

where $\bar{l} = l + 1/2$, $l = i$, j, or k. δ_u ($u = x$, y, or z) are central-difference operators defined in (3), and Δt, Δx, Δy, and Δz are time step and spatial steps along x, y, and z directions, respectively. Note that F stands for possible field components and that $a \in [0, 1/4]$ is the weighting factor. When $a = 0$, the above formulations are reduced to the conventional ADI-FDTD scheme. Superscript $m = n$, $n + 1/2$, or $n + 1$, representing time sequences of the field points, and subscripts

$\varsigma = i$ or $i + 1/2$, $\xi = j$ or $j + 1/2$, $\zeta = k$ or $k + 1/2$, denoting spatial indexes.

$$\delta_x F^m_{\varsigma,\xi,\zeta} = \left[\begin{array}{l} (1-4a) \cdot \left(F^m_{\varsigma+1/2,\xi,\zeta} - F^m_{\varsigma-1/2,\xi,\zeta} \right) \\ +a \cdot \left(F^m_{\varsigma+1/2,\xi,\zeta+1} - F^m_{\varsigma-1/2,\xi,\zeta+1} \right) \\ +a \cdot \left(F^m_{\varsigma+1/2,\xi,\zeta-1} - F^m_{\varsigma-1/2,\xi,\zeta-1} \right) \\ +a \cdot \left(F^m_{\varsigma+1/2,\xi+1,\zeta} - F^m_{\varsigma-1/2,\xi+1,\zeta} \right) \\ +a \cdot \left(F^m_{\varsigma+1/2,\xi-1,\zeta} - F^m_{\varsigma-1/2,\xi-1,\zeta} \right) \end{array} \right] \Big/ \Delta x$$

$$\delta_y F^m_{\varsigma,\xi,\zeta} = \left[\begin{array}{l} (1-4a) \cdot \left(F^m_{\varsigma,\xi+1/2,\zeta} - F^m_{\varsigma,\xi-1/2,\zeta} \right) \\ +a \cdot \left(F^m_{\varsigma+1,\xi+1/2,\zeta} - F^m_{\varsigma+1,\xi-1/2,\zeta} \right) \\ +a \cdot \left(F^m_{\varsigma-1,\xi+1/2,\zeta} - F^m_{\varsigma-1,\xi-1/2,\zeta} \right) \\ +a \cdot \left(F^m_{\varsigma,\xi+1/2,\zeta+1} - F^m_{\varsigma,\xi-1/2,\zeta+1} \right) \\ +a \cdot \left(F^m_{\varsigma,\xi+1/2,\zeta-1} - F^m_{\varsigma,\xi-1/2,\zeta-1} \right) \end{array} \right] \Big/ \Delta y \qquad (3)$$

$$\delta_z F^m_{\varsigma,\xi,\zeta} = \left[\begin{array}{l} (1-4a) \cdot \left(F^m_{\varsigma,\xi,\zeta+1/2} - F^m_{\varsigma,\xi,\zeta-1/2} \right) \\ +a \cdot \left(F^m_{\varsigma,\xi+1,\zeta+1/2} - F^m_{\varsigma,\xi+1,\zeta-1/2} \right) \\ +a \cdot \left(F^m_{\varsigma,\xi-1,\zeta+1/2} - F^m_{\varsigma,\xi-1,\zeta-1/2} \right) \\ +a \cdot \left(F^m_{\varsigma+1,\xi,\zeta+1/2} - F^m_{\varsigma+1,\xi,\zeta-1/2} \right) \\ +a \cdot \left(F^m_{\varsigma-1,\xi,\zeta+1/2} - F^m_{\varsigma-1,\xi,\zeta-1/2} \right) \end{array} \right] \Big/ \Delta z$$

After similar algebraic manipulation mentioned in [15], (1a)–(1c) and (2a)–(2c) can be further simplified for efficient computations, as shown in (4) and (5), respectively. Here $\alpha_u|_r^h$, $\beta_u|_s^h$, $\gamma_u|_t^h$ ($u = x$, y, or z; $h = 1$ or 2), and τ are coefficients relating to the electromagnetic attributes of the area considered. For reference, they are listed in Appendix A. Presume that $h = 1$ represents advancing time step from nth to $(n+1/2)$th, and $h = 2$ from $(n+1/2)$th to $(n+1)$th. $N_1 - N_3$ equal to 39, 48, and 10, respectively, denoting the number of field points involved in a computing unit.

$$\sum_{r=1}^{N_1} \alpha_x \left.\right|_r^1 \cdot E_x \left.\right|_r^{n+1/2} = \sum_{s=1}^{N_2} \beta_x \left.\right|_s^1 \cdot E_z \left.\right|_s^n + \sum_{t=1}^{N_3} \gamma_x \left.\right|_t^1 \cdot H_y \left.\right|_t^n$$

$$- \sum_{t=1}^{N_3} \gamma_x \left.\right|_t^1 \cdot H_z \left.\right|_t^n - \tau \cdot E_x \left.\right|_{center}^n$$

$$\sum_{r=1}^{N_1} \alpha_y \left.\right|_r^1 \cdot E_y \left.\right|_r^{n+1/2} = \sum_{s=1}^{N_2} \beta_y \left.\right|_s^1 \cdot E_x \left.\right|_s^n + \sum_{t=1}^{N_3} \gamma_y \left.\right|_t^1 \cdot H_z \left.\right|_t^n$$
$$- \sum_{t=1}^{N_3} \gamma_y \left.\right|_t^1 \cdot H_x \left.\right|_t^n - \tau \cdot E_y \left.\right|_{center}^n \qquad (4)$$

$$\sum_{r=1}^{N_1} \alpha_z \left.\right|_r^1 \cdot E_z \left.\right|_r^{n+1/2} = \sum_{s=1}^{N_2} \beta_z \left.\right|_s^1 \cdot E_y \left.\right|_s^n + \sum_{t=1}^{N_3} \gamma_z \left.\right|_t^1 \cdot H_x \left.\right|_t^n$$
$$- \sum_{t=1}^{N_3} \gamma_z \left.\right|_t^1 \cdot H_y \left.\right|_t^n - \tau \cdot E_z \left.\right|_{center}^n$$

$$\sum_{r=1}^{N_1} \alpha_x \left.\right|_r^2 \cdot E_x \left.\right|_r^{n+1} = \sum_{s=1}^{N_2} \beta_x \left.\right|_s^2 \cdot E_y \left.\right|_s^{n+1/2} + \sum_{t=1}^{N_3} \gamma_x \left.\right|_t^2 \cdot H_z \left.\right|_t^{n+1/2}$$
$$- \sum_{t=1}^{N_3} \gamma_x \left.\right|_t^2 \cdot H_y \left.\right|_t^{n+1/2} - \tau \cdot E_x \left.\right|_{center}^{n+1/2}$$

$$\sum_{r=1}^{N_1} \alpha_y \left.\right|_r^2 \cdot E_y \left.\right|_r^{n+1} = \sum_{s=1}^{N_2} \beta_y \left.\right|_s^2 \cdot E_z \left.\right|_s^{n+1/2} + \sum_{t=1}^{N_3} \gamma_y \left.\right|_t^2 \cdot H_x \left.\right|_t^{n+1/2}$$
$$- \sum_{t=1}^{N_3} \gamma_y \left.\right|_t^2 \cdot H_z \left.\right|_t^{n+1/2} - \tau \cdot E_y \left.\right|_{center}^{n+1/2} \qquad (5)$$

$$\sum_{r=1}^{N_1} \alpha_z \left.\right|_r^2 \cdot E_z \left.\right|_r^{n+1} = \sum_{s=1}^{N_2} \beta_z \left.\right|_s^2 \cdot E_x \left.\right|_s^{n+1/2} + \sum_{t=1}^{N_3} \gamma_z \left.\right|_t^2 \cdot H_y \left.\right|_t^{n+1/2}$$
$$- \sum_{t=1}^{N_3} \gamma_z \left.\right|_t^2 \cdot H_x \left.\right|_t^{n+1/2} - \tau \cdot E_z \left.\right|_{center}^{n+1/2}$$

To help understand the corresponding relation between the numbered unknowns and their spatial positions in a computing unit, as an example, the $E_x \left.\right|_r^{n+1/2}$'s in the first advancement of a time step is shown in Figure 2. As the computing unit is a quadrangular, care must be taken in dealing with the iterative equations of field points on the edge of the simulation area.

In (4) and (5), field components on the right-hand side are of known values at the previous time steps, while on the left-hand side are of the same field components, but within a computing unit. By traversing the computing unit around the whole area under consideration, (4) and (5) become a system of linear equations with
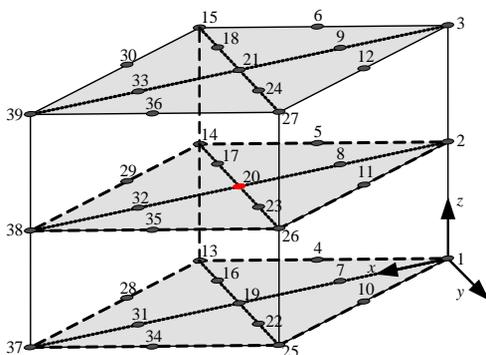
Figure 2. The relative position of the numbered unknown $E_x|_r^{n+1/2}$'s in a computing unit. Particularly, the point numbered 20 in the center of the computing unit represents $E_x|_{20}^{n+1/2}$.

the diagonally banded coefficient matrix. By solving the simultaneous linear equations of (4) and (5), the values of electric field components at $(n+1/2)$th and $(n+1)$th time step can be obtained, respectively. Once done, magnetic-field components can be calculated directly from (1d)–(1f) and (2d)–(2f) with the electric field components already updated.

2.2. Numerical Stability Analysis

Following the stability analysis procedure in [15], assume the spatial frequencies of numerical waves along x, y, and z directions are k_x, k_y, and k_z, respectively, thus a field component in the spectral domain can be expressed as

$$\phi|_{i,j,k}^n = \phi^n \cdot \exp\left[-j\left(k_x i_x \Delta x + k_y i_y \Delta y + k_z i_z \Delta z\right)\right] \tag{6}$$

where $j = \sqrt{-1}$, ϕ^n denotes the amplitude of an electromagnetic field component at the nth time step.

Substitute (6) into (1) and (2), combine these equations, eliminate the field components at $(n+1/2)$th step and rewrite them into matrix form, one gets

$$\mathbf{C}^{n+1} = \mathbf{\Lambda} \cdot \mathbf{C}^n \tag{7}$$

where $\mathbf{C}^n = [E_x^n \ E_y^n \ E_z^n \ H_x^n \ H_y^n \ H_z^n]^T$ contains six field components at the nth time step, and $\mathbf{\Lambda}$ is the amplification matrix which can be computed with the help of Maple. The eigenvalues of $\mathbf{\Lambda}$ can be obtained as

$$\lambda_1 = \lambda_2 = 1$$

$$\lambda_3 = \lambda_4 = \frac{\sqrt{K_1^2 - K_2^2} + jK_2}{K_1}$$

$$\lambda_5 = \lambda_6 = \frac{\sqrt{K_1^2 - K_2^2} - jK_2}{K_1}$$

K_1 and K_2 are coefficients listed in Appendix A. It can be easily demonstrated that the eigenvalues have a magnitude of unity. According to the Von Neumann stability analysis theory, neutral stability is maintained so QI-ADI-FDTD is unconditionally stable in any case.

2.3. Numerical Dispersion Relationship

To obtain the numerical dispersion relationship, a monochromatic wave with angular frequency ω is assumed as $u_n = ue^{j\omega n \Delta t}$, thus (7) can be expressed in the following way [29].

$$\left(e^{j\omega n\Delta t}\mathbf{I} - \mathbf{\Lambda}\right) \cdot \mathbf{C} = 0 \tag{8}$$

where $\mathbf{I}$ is a 6×6 identity matrix. Note that the determinant of the coefficient matrix is zero since vector $\mathbf{C}$ is a nontrivial solution to the homogeneous system of equations. For simplicity, a uniform grid is assumed, that is, $\Delta x = \Delta y = \Delta z = \Delta$. Thus the numerical dispersion relationship of QI-ADI-FDTD can be obtained as

$$T^2 SX^2 SY^2 SZ^2 P^2 Q^2 R^2 S^6 - \left(SX^2 SY^2 R^2 P^2\right.$$
$$+ SY^2 SZ^2 P^2 Q^2 + SZ^2 SX^2 Q^2 R^2\right) S^4$$
$$- \left(SX^2 R^2 + SY^2 P^2 + SZ^2 Q^2\right) S^2 + T^2 = 0 \tag{9}$$

where $T = \tan(\pi S/N_\lambda)$, $SX = \sin(k_x \cdot \Delta/2)$, $SY = \sin(k_y \cdot \Delta/2)$, $SZ = \sin(k_z \cdot \Delta/2)$, $P = (1 - 4a) + 2a\cos(k_z\Delta z) + 2a\cos(k_x\Delta x)$, $Q = (1 - 4a) + 2a\cos(k_x\Delta x) + 2a\cos(k_y\Delta y)$, $R = (1 - 4a) + 2a\cos(k_y\Delta y) + 2a\cos(k_z\Delta z)$. $S = c\Delta t/\Delta$ is the Courant number, and $N_\lambda = \lambda/\Delta$ is the grid sampling resolution in space cells per wavelength.

2.4. Determination of Optimal Weighting Factor

It is easily seen in (9) that a is a function of azimuth angle, grid size and time step. To investigate the extent a is affected by the variation of azimuth angle and grid size, a fixed grid size is assumed. As the underlying dispersion relation (9) is a transcendental equation, a useful approach to obtain sample values of a is to apply Newton's method [30].

For a uniform, cubic, three-dimensional grid, the critical Courant number $S = 1/\sqrt{3}$. As seen in Figure 3, for a grid size smaller than $\lambda/10$, the weighting factor changes less than 8×10^{-3} even when S gets
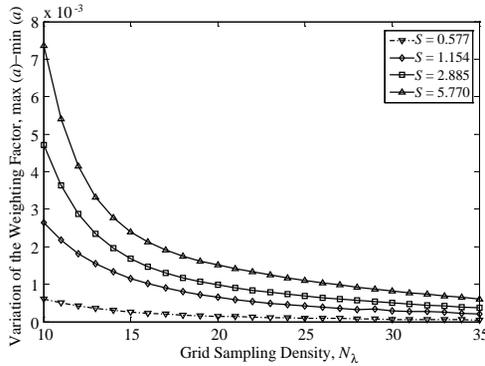
Figure 3. Difference between the maximal and the minimal weighting factor a while azimuth angle (θ, φ) and time step Δt vary and grid sampling density N_λ unchanged.

10 times as large as the critical Courant number, thus the optimal a can be empirically estimated as the average of all the weighting factors over the azimuth angles [28]. Further, to find the "true value" of the optimal a, an optimizing model targeting at smallest numerical dispersion fluctuation should be built, which is a more complex procedure.

Once the estimated optimal weighting factor a is obtained, a revision procedure on the anisotropic numerical space should be performed: 1) choose the fastest phase velocity, which propagates along the grid main diagonals, to be the exact one, thus no phase velocities exceed light speed c after revision; 2) equate the wave number k in (9) to k_{exact} and substitute c with c/sf, where sf is the scaling factor; 3) work out the value of sf and revise the electromagnetic attributes with $\varepsilon' = sf \times \varepsilon$ and $\mu' = sf \times \mu$.

3. DISCUSSION ON NUMERICAL DISPERSION

In this section, the numerical dispersion characteristics of both QI-ADI-FDTD and conventional ADI-FDTD methods will be investigated and compared in detail. The normalized phase velocity as well as dispersion error will be used to characterize the numerical dispersion of different methods.

3.1. Numerical Dispersion Characteristics versus Propagation Angle

In this study, N_λ and S_N (already normalized to critical Courant number) are set to 10 and 2, respectively. Therefore, it can be worked

out that $a = 0.1162$ and $sf = 0.9426$. To measure the deviation of the numerical phase velocity v_p from its physical value c, the maximum phase velocity error $|1 - v_p/c|$ is defined and denoted as E_{MPV} for simplicity. In addition, to describe the difference between the maximum and minimum normalized phase velocities for different propagation directions at a particular wavelength, the anisotropic error of phase velocity $(v_{p,\max} - v_{p,\min})/c$ is defined and denoted as E_{APV}.

Due to the wide range of normalized phase velocity variations, v_p and E_{MPV} within the whole range of φ for cases $\theta = \pi/8$, $\pi/4$, $3\pi/8$, and $\pi/2$ will be analyzed, respectively.

In Figure 4 and Figure 5 it is intuitively seen that the numerical phase velocity of QI-ADI-FDTD is much closer to the theoretical value than the conventional ADI-FDTD method over the range $0 \leq \varphi \leq \pi/2$. More specifically, in cases $\theta = \pi/4$, $3\pi/8$, and $\pi/2$, both methods get their fastest phase velocities when $\varphi = \pi/4$ and slowest when $\varphi = 0$ or $\pi/2$, and E_{MPV} occurs when $\varphi = 0$ or $\pi/2$; in the case $\theta = \pi/8$, the same conclusions can be drawn for ADI-FDTD, whereas for QI-ADI-FDTD, the opposite conclusions are true. Also, the anisotropic error is greater in ADI-FDTD than in QI-ADI-FDTD method.
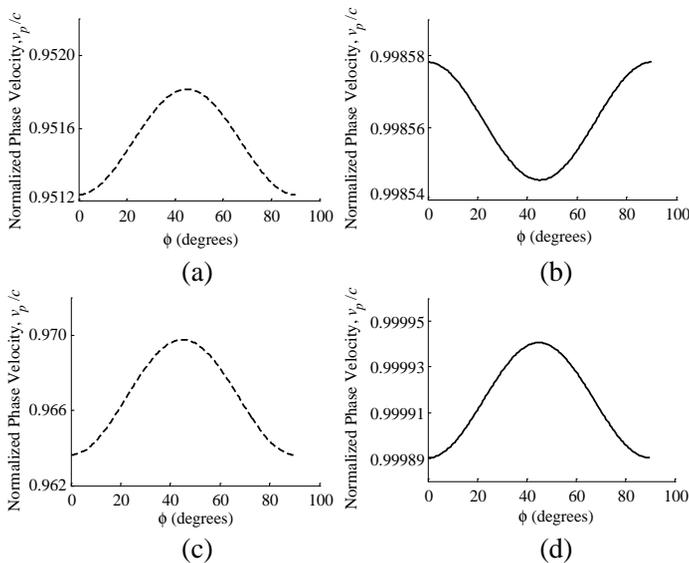

Figure 4. Normalized phase velocity of different methods versus wave propagation angle φ while $\theta = \pi/8$ and $\pi/4$. (a) ADI-FDTD $\theta = \pi/8$. (b) QI-ADI-FDTD $\theta = \pi/8$. (c) ADI-FDTD $\theta = \pi/4$. (d) QI-ADI-FDTD $\theta = \pi/4$.

Figure 5. Normalized phase velocity of different methods versus wave propagation angle φ while $\theta = 3\pi/8$ and $\pi/2$. (a) ADI-FDTD $\theta = 3\pi/8$. (b) QI-ADI-FDTD $\theta = 3\pi/8$. (c) ADI-FDTD $\theta = \pi/2$. (d) QI-ADI-FDTD $\theta = \pi/2$.
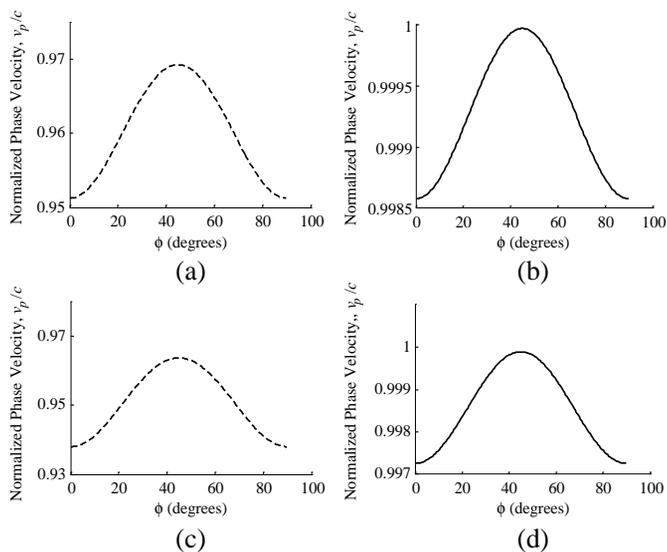
For the four cases analyzed above, the values of E_{MPV} and E_{APV} for both methods are listed in Table 1. For all propagation angles, the estimated values of E_{MPV} and E_{APV} for both methods are listed in Table 2. These comparisons show that for QI-ADI-FDTD, E_{MPV} and E_{APV} are tens of times less than those of ADI-FDTD, thus QI-ADI-FDTD performs better than conventional ADI-FDTD in terms of numerical dispersion characteristics versus propagation angles.

Table 1. Values of E_{MPV} and E_{APV} for both methods in four cases.

Propagation directions	ADI-FDTD		QI-ADI-FDTD	
	E_{MPV}	E_{APV}	E_{MPV}	E_{APV}
$\theta = \pi/8$	4.876%	0.058%	0.145%	0.003%
$\theta = \pi/4$	3.635%	0.611%	0.011%	0.005%
$\theta = 3\pi/8$	4.876%	1.799%	0.142%	0.139%
$\theta = \pi/2$	6.202%	2.567%	0.274%	0.263%

Table 2. Estimated values of E_{MPV} and E_{APV} for both methods in all propagation angles.

Method	ADI-FDTD	QI-ADI-FDTD
E_{MPV}	6.202%	0.274%
E_{APV}	3.375%	0.269%

3.2. Maximum Error and Anisotropic Error of Phase Velocity versus Time Step

In this part, E_{MPV} and E_{APV} with different time steps will be investigated. N_λ is set to 50 and S_N varies from 1 to 25. As for QI-ADI-FDTD, a in different time steps is almost constant around 0.1135, and sf varies from 0.9965 to 0.8237.

From Figure 6 and Figure 7 one can draw the following conclusions: 1) With time steps going up, both methods' E_{MPV} and E_{APV} get larger; 2) E_{MPV} and E_{APV} of QI-ADI-FDTD are smaller than the corresponding indicators of ADI-FDTD; 3) QI-ADI-FDTD method shows a significant reduction of E_{MPV} and E_{APV} when compared with ADI-FDTD at larger time steps, thus the advantage in numerical dispersion characteristics is more obvious when time step gets larger. In other words, for a given numerical dispersion error, QI-ADI-FDTD can take a time step larger than that of ADI-FDTD, leading to a saving of computation time.
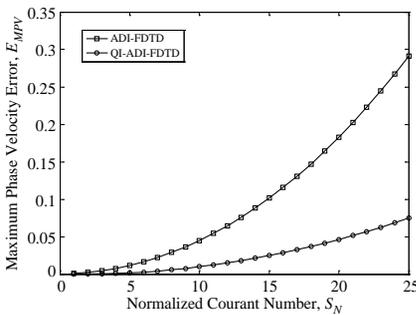

Figure 6. Comparisons of E_{MPV} in conventional ADI-FDTD and QI-ADI-FDTD method versus different time steps.
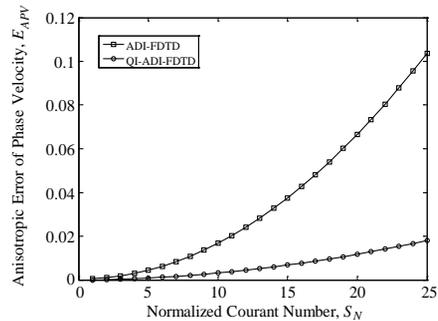
Figure 7. Comparisons of E_{APV} in conventional ADI-FDTD and QI-ADI-FDTD method versus different time steps.

3.3. Maximum Error and Anisotropic Error of Phase Velocity versus Grid Sampling Density

In this part, E_{MPV} and E_{APV} of both methods with different grid sampling densities will be investigated. The reference S_N is set to 4. As for QI-ADI-FDTD, a and sf in different grid sampling densities are given in Table 3.

Table 3. Values of weighting factor and scaling factor for grid sampling density range 10–50.

N_λ	10	15	20	25	30	35	40	45	50
a	0.1172	0.1161	0.1152	0.1146	0.1139	0.1137	0.1136	0.1135	0.1135
sf	0.8805	0.9455	0.9731	0.9826	0.9859	0.9896	0.9927	0.9944	0.9962

From Figure 8 and Figure 9 one can draw the following conclusions: 1) As grid sampling density goes up, both methods' E_{MPV} and E_{APV} get smaller; 2) QI-ADI-FDTD method shows a significant reduction of E_{MPV} and E_{APV} when compared with ADI-FDTD; 3) for grid sampling density larger than 15, E_{MPV} and E_{APV} of QI-ADI-FDTD tend to be constant, which implies that QI-ADI-FDTD is well fit for wideband frequency problems.
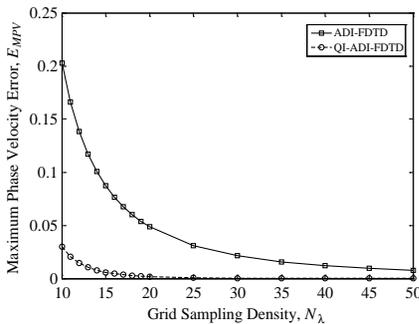

Figure 8. Comparisons of E_{MPV} in conventional ADI-FDTD and QI-ADI-FDTD method versus different grid sampling densities.
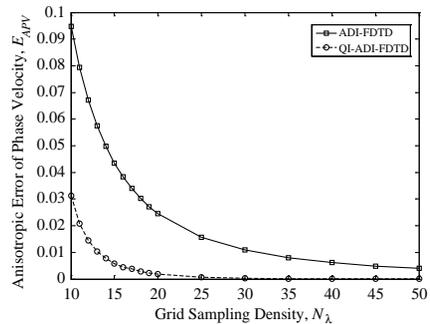
Figure 9. Comparisons of E_{APV} in conventional ADI-FDTD and QI-ADI-FDTD method versus different grid sampling densities.

4. NUMERICAL EXAMPLE

In this section, the resonant frequencies of an air-filled rectangular cavity are simulated to confirm the theory and demonstrate the

accuracy of the newly developed QI-ADI-FDTD method. For comparative purposes, conventional ADI-FDTD is also chosen to simulate the same model.

The size of rectangular cavity is selected to be $10\,\text{cm} \times 4.8\,\text{cm} \times 2\,\text{cm}$, and a uniform mesh size ($\Delta x = \Delta y = \Delta z = 2\,\text{mm}$) is chosen. For conventional ADI-FDTD and QI-ADI-FDTD methods, cases $S_N = 2$ and $S_N = 4$ are investigated. A current line source J_z with the following form is placed across from the bottom to the top at the center of the computational area.

$$J_z = \exp\left[-\frac{(t - t_0)^2}{T^2}\right], \quad T = 50\,\text{ps}; \quad t_0 = 6\,\text{T}.$$

For QI-ADI-FDTD method, $(a,\,sf)$ is set to (0.1146, 0.9900) and (0.1146, 0.9826) for each case. Weighting factor a is initially devised to be optimal at frequency $f = 6\,\text{GHz}$.

The E_z component at observation point (5 cm, 1.2 cm, 1 cm) is output. Figure 10 shows the waveform of time-domain electric field component E_z obtained by the two methods in different time steps. From Figure 10 it can be seen that the results of QI-ADI-FDTD agree well with the conventional ADI-FDTD method. The resonant frequencies computed by the two methods are depicted in Figure 11 and numerically shown in Table 4. From Figure 11 and Table 4 it is evident that the results computed by QI-ADI-FDTD method present better agreement with the analytical values than ADI-FDTD.

These simulations are performed on a Dell vostro 260 s PC. CPU Time and memory requirements of the two methods in different time
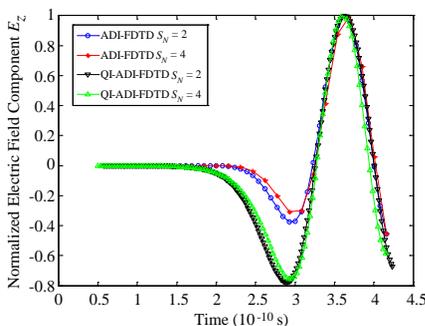

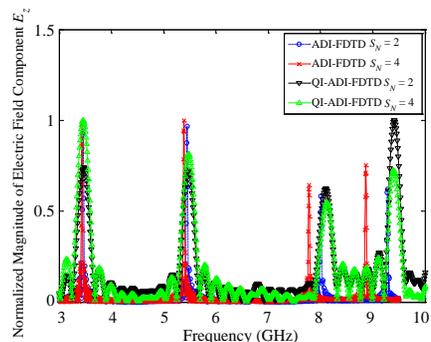**Figure 10.** Time-domain electric field component E_z at the observation point.

Figure 11. Resonant frequencies of the air-filled rectangular cavity.

Table 4. Resonant frequencies of air-filled rectangular cavity.

Method		TE_{110}		TE_{310}		TE_{011}		TE_{021}	
		Results (GHz)	Relative Error	Results (GHz)	Relative Error	Results (GHz)	Relative Error	Results (GHz)	Relative Error
Analytic Results		3.464	-	5.475	-	8.119	-	9.756	-
ADI-FDTD	$S=2$	3.456	0.23%	5.447	0.51%	8.008	1.37%	9.276	4.92%
	$S=4$	3.437	0.78%	5.385	1.64%	7.779	4.19%	8.865	9.13%
QI-ADI-FDTD	$S=2$	3.462	0.06%	5.470	0.09%	8.111	0.09%	9.415	3.49%
	$S=4$	3.461	0.09%	5.468	0.13%	8.127	0.10%	9.406	3.59%

Table 5. Computational requirement comparisons of conventional ADI-FDTD and QI-ADI-FDTD method.

Method		Steps	CPU Time (s)	Memory (MB)
ADI-FDTD	$S=2$	5000	141	12.5
	$S=4$	2500	71	12.4
QI-ADI-FDTD	$S=2$	5000	268	25.8
	$S=4$	2500	136	25.6

steps are shown in Table 5. Under the same circumstances, computing time and memory requirements of QI-ADI-FDTD are approximately 1.9 and 2.0 times of the corresponding indexes of ADI-FDTD. As is known that for QI-ADI-FDTD, all the same electric field points are simultaneously computed, thus longer time and larger storage space are needed in solving diagonal matrixes. However, when combined with Table 5 it can be concluded that to achieve the same computational accuracy, a larger time step and coarser mesh can be used for QI-ADI-FDTD; consequently, the computational requirements will be less.

5. CONCLUSIONS

In this paper, the quasi isotropic ADI-FDTD method is formulated, and its numerical dispersion relationship is analytically studied and numerically investigated. It is found that QI-ADI-FDTD can not only maintain the unconditionally stable advantage, but also achieve better numerical dispersion characteristics with a simple correction scheme. The numerical simulation shows that the proposed method can improve computational accuracy of the conventional ADI-FDTD method. Therefore, to achieve the same computational accuracy, the time step of QI-ADI-FDTD can be set larger, in which case the computation time and memory can be saved.

ACKNOWLEDGMENT

APPENDIX A.

To save space, only $\alpha_x|_r^1$, $\beta_x|_s^1$ and $\gamma_x|_t^1$ will be given. Based on the coordinate-symmetry principle, $\alpha_u|_r^1$, $\beta_u|_s^1$, $\gamma_u|_t^1$ ($u = y$ or z) and coefficients in the second computing stage can be reached with similar procedures.

$$\alpha_x\,\big|_1^1 = \alpha_x\,\big|_3^1 = \alpha_x\,\big|_{13}^1 = \alpha_x\,\big|_{15}^1 = \alpha_x\,\big|_{25}^1$$
$$= \alpha_x\,\big|_{27}^1 = \alpha_x\,\big|_{37}^1 = \alpha_x\,\big|_{39}^1 = g_1 \cdot Cb \cdot Db \tag{A1}$$

$$\alpha_x\,\big|_2^1 = \alpha_x\,\big|_{14}^1 = \alpha_x\,\big|_{26}^1 = \alpha_x\,\big|_{38}^1 = -2g_1 \cdot Cb \cdot Db \tag{A2}$$

$$\alpha_x\,\big|_4^1 = \alpha_x\,\big|_6^1 = \alpha_x\,\big|_{10}^1 = \alpha_x\,\big|_{12}^1 = \alpha_x\,\big|_{28}^1$$
$$= \alpha_x\,\big|_{30}^1 = \alpha_x\,\big|_{34}^1 = \alpha_x\,\big|_{36}^1 = 2g_1 \cdot Cb \cdot Db \tag{A3}$$

$$\alpha_x\,\big|_5^1 = \alpha_x\,\big|_{11}^1 = \alpha_x\,\big|_{29}^1 = \alpha_x\,\big|_{35}^1 = -4g_1 \cdot Cb \cdot Db \tag{A4}$$

$$\alpha_x\,\big|_7^1 = \alpha_x\,\big|_9^1 = \alpha_x\,\big|_{16}^1 = \alpha_x\,\big|_{18}^1 = \alpha_x\,\big|_{22}^1 = \alpha_x\,\big|_{24}^1$$
$$= \alpha_x\,\big|_{31}^1 = \alpha_x\,\big|_{33}^1 = -2g_2 \cdot Cb \cdot Db \tag{A5}$$

$$\alpha_x\,\big|_8^1 = \alpha_x\,\big|_{17}^1 = \alpha_x\,\big|_{23}^1 = \alpha_x\,\big|_{32}^1 = 4g_2 \cdot Cb \cdot Db \tag{A6}$$

$$\alpha_x\,\big|_{19}^1 = \alpha_x\,\big|_{21}^1 = \left(20 - 8/a + 1/a^2\right) g_1 \cdot Cb \cdot Db \tag{A7}$$

$$\alpha_x\,\big|_{20}^1 = -\left[1 + 2\left(20 - 8/a + 1/a^2\right) \cdot g_1 \cdot Cb \cdot Db\right] \tag{A8}$$

$$\beta_x\,\big|_1^1 = \beta_x\,\big|_3^1 = \beta_x\,\big|_7^1 = \beta_x\,\big|_9^1 = \beta_x\,\big|_{11}^1 = \beta_x\,\big|_{19}^1$$
$$= \beta_x\,\big|_{23}^1 = \beta_x\,\big|_{26}^1 = \beta_x\,\big|_{30}^1 = \beta_x\,\big|_{38}^1 = \beta_x\,\big|_{40}^1$$
$$= \beta_x\,\big|_{42}^1 = \beta_x\,\big|_{46}^1 = \beta_x\,\big|_{48}^1 = g_1 \cdot Cb \cdot Db \tag{A9}$$

$$\beta_x\,\big|_2^1 = \beta_x\,\big|_6^1 = \beta_x\,\big|_8^1 = \beta_x\,\big|_{10}^1 = \beta_x\,\big|_{14}^1 = \beta_x\,\big|_{22}^1$$
$$= \beta_x\,\big|_{24}^1 = \beta_x\,\big|_{25}^1 = \beta_x\,\big|_{27}^1 = \beta_x\,\big|_{35}^1 = \beta_x\,\big|_{39}^1$$
$$= \beta_x\,\big|_{41}^1 = \beta_x\,\big|_{43}^1 = \beta_x\,\big|_{47}^1 = -g_1 \cdot Cb \cdot Db \tag{A10}$$

$$\beta_x \left.\right|_4^1 = \beta_x \left.\right|_{15}^1 = \beta_x \left.\right|_{34}^1 = \beta_x \left.\right|_{45}^1 = -\left(5 - 1/a\right) \cdot g_1 \cdot Cb \cdot Db \quad \text{(A11)}$$

$$\beta_x \left.\right|_5^1 = \beta_x \left.\right|_{18}^1 = \beta_x \left.\right|_{31}^1 = \beta_x \left.\right|_{44}^1 = \left(5 - 1/a\right) \cdot g_1 \cdot Cb \cdot Db \quad \text{(A12)}$$

$$\beta_x \left.\right|_{12}^1 = \beta_x \left.\right|_{20}^1 = \beta_x \left.\right|_{29}^1 = \beta_x \left.\right|_{37}^1 = -2\left(5 - 1/a\right) \cdot g_1 \cdot Cb \cdot Db \quad \text{(A13)}$$

$$\beta_x \left.\right|_{13}^1 = \beta_x \left.\right|_{21}^1 = \beta_x \left.\right|_{28}^1 = \beta_x \left.\right|_{36}^1 = 2\left(5 - 1/a\right) \cdot g_1 \cdot Cb \cdot Db \quad \text{(A14)}$$

$$\beta_x \left.\right|_{16}^1 = \beta_x \left.\right|_{33}^1 = \left(27 - 10/a + 1/a^2\right) \cdot g_1 \cdot Cb \cdot Db \quad \text{(A15)}$$

$$\beta_x \left.\right|_{17}^1 = \beta_x \left.\right|_{32}^1 = -\left(27 - 10/a + 1/a^2\right) \cdot g_1 \cdot Cb \cdot Db \quad \text{(A16)}$$

$$\gamma_x \left.\right|_1^1 = -\gamma_x \left.\right|_2^1 = -(4a - 1) \cdot Cb/\Delta \quad \text{(A17)}$$

$$\gamma_x \left.\right|_3^1 = \gamma_x \left.\right|_5^1 = \gamma_x \left.\right|_7^1 = \gamma_x \left.\right|_9^1 = a \cdot Cb/\Delta \quad \text{(A18)}$$

$$\gamma_x \left.\right|_4^1 = \gamma_x \left.\right|_6^1 = \gamma_x \left.\right|_8^1 = \gamma_x \left.\right|_{10}^1 = -a \cdot Cb/\Delta \quad \text{(A19)}$$

$$\tau = \frac{4\varepsilon - \sigma \cdot \Delta t}{4\varepsilon + \sigma \cdot \Delta t} \quad \text{(A20)}$$

where $g_1 = a^2/\Delta^2$, $g_2 = a(4a - 1)^2/\Delta^2$, $Cb = 2\Delta t/(4\varepsilon + \sigma \cdot \Delta t)$, $Db = \Delta t/(2\mu)$.

K_1 and K_2 in Section 2.2 are expressed as

$$K_1 = \left\lfloor R^2 SX^2 \left(\Delta t\right)^2 + \mu\varepsilon \left(\Delta x\right)^2 \right\rfloor \cdot \left\lfloor P^2 SY^2 \left(\Delta t\right)^2 + \mu\varepsilon \left(\Delta y\right)^2 \right\rfloor$$
$$\cdot \left\lfloor Q^2 SZ^2 \left(\Delta t\right)^2 + \mu\varepsilon \left(\Delta z\right)^2 \right\rfloor \quad \text{(A21)}$$

$$K_2 = 2 \sqrt{ \mu\varepsilon \left(\Delta t\right)^2 \begin{bmatrix} \mu^3 \varepsilon^3 \Delta x \Delta y \Delta z \\ + Q^2 P^2 R^2 SX^2 SY^2 SZ^2 \left(\Delta t\right)^6 \end{bmatrix} \cdot \begin{bmatrix} Q^2 R^2 SZ^2 SX^2 \Delta y \left(\Delta t\right)^2 + R^2 P^2 SX^2 SY^2 \Delta z \left(\Delta t\right)^2 \\ + P^2 Q^2 SY^2 SZ^2 \Delta x \left(\Delta t\right)^2 + \mu\varepsilon R^2 SX^2 \Delta y \Delta z \\ + \mu\varepsilon P^2 SY^2 \Delta z \Delta x + \mu\varepsilon Q^2 SZ^2 \Delta x \Delta y \end{bmatrix} } \quad \text{(A22)}$$

REFERENCES

1. Dai, J., Z. Z. Chen, D. L. Su, and X. Y. Zhao, "Stability analysis and improvement of the conformal ADI-FDTD methods," *IEEE Trans. on Antennas Propag.*, Vol. 59, No. 6, 2248–2258, Jun. 2011.

2. Wang, J.-B., B.-H. Zhou, L.-H. Shi, C. Gao, and B. Chen, "A novel 3-D weakly conditionally stable FDTD algorithm," *Progress In Electromagnetics Research*, Vol. 130, 525–540, 2012.

3. Mao, Y., B. Chen, H.-Q. Liu, J.-L. Xia, and J.-Z. Tang, "A hybrid implicit-explicit spectral FDTD scheme for oblique incidence problems on periodic structures," *Progress In Electromagnetics Research*, Vol. 128, 153–170, 2012.

4. Wang, W., P.-G. Liu, and Y.-J. Qin, "An unconditional stable 1D-FDTD method for modeling transmission lines based on precise split-step scheme," *Progress In Electromagnetics Research*, Vol. 135, 245–260, 2013.

5. Kong, Y.-D., Q.-X. Chu, and R.-L. Li, "Two efficient unconditionally-stable four-stages split-step FDTD methods with low numerical dispersion," *Progress In Electromagnetics Research B*, Vol. 48, 1–22, 2013.

6. Heh, D. Y. and E. L. Tan, "Unified efficient fundamental ADI-FDTD schemes for lossy media," *Progress In Electromagnetics Research B*, Vol. 32, 217–242, 2011.

7. Gao, J.-Y. and H.-X. Zheng, "One-step leapfrog ADI-FDTD method for lossy media and its stability analysis," *Progress In Electromagnetics Research Letters*, Vol. 40, 49–60, 2013.

8. Dai, J., D. L. Su, and X. Y. Zhao, "A scheme of lightning pulse source for the FDTD analysis of near-field interaction with airplane," *8th International Symposium on Antennas, Propagation and EM Theory, ISAPE 2008*, 843–846, Beijing, China, Nov. 2008.

9. Vaccari, A., A. Cala' Lesina, L. Cristoforetti, and R. Pontalti, "Parallel implementation of a 3D subgridding FDTD algorithm for large simulations," *Progress In Electromagnetics Research*, Vol. 120, 263–292, 2011.

10. Izadi, M., M. Z. A. Ab Kadir, and C. Gomes, "Evaluation of electromagnetic fields associated with inclined lightning channel using second order FDTD-hybrid methods," *Progress In Electromagnetics Research*, Vol. 117, 209–236, 2011.

11. Xiong, R., B. Chen, J.-J. Han, Y.-Y. Qiu, W. Yang, and Q. Ning, "Transient resistance analysis of large grounding systems using the FDTD method," *Progress In Electromagnetics Research*, Vol. 132, 159–175, 2012.

12. Markovich, D. L., K. S. Ladutenko, and P. A. Belov, "Performance of FDTD method CPU implementations for simulation of electromagnetic processes," *Progress In Electromagnetics Research*, Vol. 139, 655–670, 2013.

13. Ashutosh and P. K. Jain, "FDTD analysis of the dispersion characteristics of the metal PBG structures," *Progress In Electromagnetics Research B*, Vol. 39, 71–88, 2012.

14. Guo, X.-M., Q.-X. Guo, W. Zhao, and W. Yu, "Parallel FDTD simulation using numa acceleration technique," *Progress In Electromagnetics Research Letters*, Vol. 28, 1–8, 2012.

15. Zheng, F. H., Z. Z. Chen, and J. Z. Zhang, "Toward the

development of a three-dimensional unconditionally stable finite-difference time-domain method," *IEEE Trans. on Microwave Theory Tech.*, Vol. 48, No. 9, 1550–1558, Sep. 2000.

16. Wang, M. H., Z. Wang, and J. Chen, "A parameter optimized ADI-FDTD method," *IEEE Antennas Wireless Propag. Lett.*, Vol. 2, No. 1, 118–121, 2003.

17. Fu, W. M. and E. L. Tan, "A parameter optimized ADI-FDTD method based on the (2, 4) stencil," *IEEE Trans. on Antennas Propag.*, Vol. 54, No. 6, 1836–1842, Jun. 2006.

18. Ahmed, I. and Z. Chen, "Dispersion-error optimized ADI FDTD," *Proc. IEEE MTT-S Int. Microw. Symp. Dig.*, 173–176, Jun. 2006.

19. Juntunen, J. S. and T. D. Tsiboukis, "Reduction of numerical dispersion in FDTD method through artificial anisotropy," *IEEE Trans. on Microwave Theory Tech.*, Vol. 48, No. 4, 582–588, Apr. 2000.

20. Zheng, H. X. and K. W. Leung, "An efficient method to reduce the numerical dispersion in the ADI-FDTD," *IEEE Trans. on Microwave Theory Tech.*, Vol. 53, No. 7, 2295–2301, Jul. 2005.

21. Zhang, Y., S. W. Lü, and J. Zhang, "Reduction of numerical dispersion of 3-D higher order alternating-direction-implicit finite difference time-domain method with artificial anisotropy," *IEEE Trans. on Microwave Theory Tech.*, Vol. 57, No. 10, 2416–2428, Oct. 2009.

22. Lee, J. and B. Fornberg, "A split step approach for the 3-D Maxwell's equations," *J. Comput. Appl. Math.*, Vol. 158, 485–505, Mar. 2003.

23. Shibayama, J., M. Muraki, J. Yamauchi, and H. Nakano, "Efficient implicit FDTD algorithm based on locally one-dimensional scheme," *Electron. Lett.*, Vol. 41, No. 19, 1046–1047, Sep. 2005.

24. Fu, W. and E. L. Tan, "Development of split-step FDTD method with higher-order spatial accuracy," *Electron. Lett.*, Vol. 40, No. 20, 1252–1253, Sep. 2004.

25. Kong, Y. D. and Q. X. Chu, "High-order split-step unconditionally-stable FDTD methods and numerical analysis," *IEEE Trans. on Antennas Propag.*, Vol. 59, No. 9, 3280–3289, Sep. 2011.

26. Kong, Y. D. and Q. X. Chu, "Reduction of numerical dispersion of the six-stages split-step unconditionally-stable FDTD method with controlling parameters," *Progress In Electromagnetics Research*, Vol. 122, 175–196, 2012.

27. Liu, Q. F., Z. Chen, and W. Y. Yin, "An arbitrary order LOD-FDTD method and its stability and numerical dispersion," *IEEE Trans. on Antennas Propag.*, Vol. 57, No. 8, 2409–2417, Aug. 2009.

28. Koh, I. S., H. Kim, J. M. Lee, J. G. Yook, and C. S. Pil, "Novel explicit 2-D FDTD scheme with isotropic dispersion and enhanced stability," *IEEE Trans. on Antennas Propag.*, Vol. 54, No. 11, 3505–3510, Nov. 2006.

29. Gao, L. P., "A new form of the numerical dispersion relation of ADI-FDTD for the 3D Maxwell's equations," *5th International Conference on Wireless Communications, Networking and Mobile Computing, WiCom' 09*, 24–26, Beijing, China, Sep. 2009.

30. Talflove, A., *Computational Electrodynamics: The Finite-difference Time-domain Method,* Artech House, Norwood, MA, 2000.